Frequency, Genotype, and Clinical Spectrum of Best Vitelliform Macular Dystrophy: Data From a National Center in Denmark

Bitner, Hanna; Schatz, Patrik; Mizrahi-Meissonnier, Liliana; Sharon, Dror; Rosenberg, Thomas

Published in:
American Journal of Ophthalmology

DOI:
10.1016/j.ajo.2012.02.036

2012

Frequency, genotype and clinical spectrum of Best vitelliform macular dystrophy: Data from a National center in Denmark

Hanna Bitner[1*] MSc, Patrik Schatz[2,3,4*] MD PhD, Liliana Mizrahi-Meissonnier[1] MSc, Dror Sharon[1] PhD, Thomas Rosenberg[4] MD

[1] Department of Ophthalmology, Hadassah-Hebrew University Medical Center, Jerusalem, Israel.
[2] Department of Ophthalmology, Glostrup Hospital, University of Copenhagen, Denmark.
[3] Department of Ophthalmology, Lund University Hospital, University of Lund, Sweden.
[4] National Eye Clinic, Kennedy Center, Glostrup, Denmark.
* These authors contributed equally to this work.

Short title: Best vitelliform macular dystrophy in Denmark.

Statement: Each of the coauthors has seen and agrees with each of the changes made to this manuscript in the revision and to the way his or her name is listed.
Supplemental Material available at AJO.com

Keywords; Best vitelliform macular dystrophy, prevalence, *BEST1* mutations, phenotype

Correspondence to:
Patrik Schatz, Department of Ophthalmology, Lund University Hospital, 22185 Lund, Sweden.
Telephone number: +46 46 171000. E mail: patrik.schatz@med.lu.se

Introduction

Heterozygous mutations in the Bestrophin 1 gene (*BEST1)* are the molecular basis of Best vitelliform macular dystrophy, also known as Best disease, which is inherited mainly in an autosomal dominant mode. Autosomal recessive *BEST1* mutations are usually associated with more severe retinal dystrophies, such as autosomal recessive bestrophinopathy (ARB)[1-5] and retinitis pigmentosa.[6] Best disease is considered a rare genetic disease, but the prevalence in still unknown. A previous estimate of its prevalence, carried out in Northern Sweden, arrived at 2 per 10,000.[7]

The typical manifestations and progression of Best disease through different clinical stages based on ophthalmoscopical fundus appearance has been known for decades, describing the pattern and evolution of vitelliform alterations ranging from Stage 0 with a normal fundus to Stage 4 with fibrosis or atrophy.[1] Further characterization of microstructural alterations by optical coherence tomography, fundus autofluorescence imaging and histopathology has revealed lipofuscin accumulations in and around the retinal pigment epithelium, subretinal fluid, and varying amounts of photoreceptor atrophy. In a recent paper, we found a relationship between the degree of preservation of the photoreceptor inner segment-outer segment junction in the central retina, and visual function.[8] Further understanding of the relationship between structure and function in Best disease is spurred by the recent work aiming at developing gene therapy (Guziewicz K, et al. IOVS 2011;52:ARVO E-Abstract 4378) for Canine Multifocal Retinopathy, an animal model for Best disease.[9] More specifically, there will probably exist a therapeutic window for successful gene therapy. Obviously by the time that Stage 4 has been reached, gene therapy will most likely fail to produce any effect on vision. Thus a more nuanced understanding of the relationship between structure and function in Best disease may be useful in determining which patients may be eligible for future gene therapy.

This study was initiated to estimate the prevalence of Best disease in the Danish population, and to describe its mutation spectrum. We also present a detailed analysis of retinal function and structure among Danish patients with Best disease in whom a molecular genetic diagnosis was established in the present study.

Patients and Methods:

Probands were identified from the files of the National Low Vision Eye Clinic, which offers specialized diagnostics and optical rehabilitation and is a national referral center. This retrospective, study comprised all patients examined between 1980 and 2006 including children 0-18 years of age with Snellen visual acuities 0.3 or less reported to a compulsory National registry at the clinic. Further patients were identified in a National family archive for genetic eye diseases at the National low vision eye clinic. Patients in whom a molecular genetic diagnosis was recently established (10 patients in the present study), were offered a clinical follow-up examination.

Clinical and Statistical Methods

Danish patients with Best disease who have not been described previously and in whom we recently identified causative mutations (presented herein) in *BEST1* were offered a follow-up examination including a standard clinical examination, including multifocal electroretinography (mfERG) with infrared fundus camera to monitor fixation during the recording,[10] fundus autofluorescence imaging, and spectral domain optical coherence tomography (SD-OCT) as described previously.[8] Measures of foveal thickness and maximum height of subfoveal fluid were obtained manually using calipers and were measured on horizontal transfoveal line scans.

To explore the consequences of the precipitate-like alterations at the level of the photoreceptor outer segments in terms of retinal function, we measured the extent of these changes, which coincided with the extent of subretinal fluid, along the two diagonal axes for each lesion, using manual caliper measurement on the Spectralis infrared fundus images obtained simultaneously with the SD-OCT (Fig. 1). These SD-OCT guided, fundus photographic caliper measurements of lesion size were obtained in duplicate by two independent observers. The described measures of lesion size (two for each lesion) were correlated with the extent of reduction of mfERG amplitude averages along the corresponding diagonal axes (Fig. 1). The latter were obtained as follows.

With the mfERG VERIS software, it is possible to average any combination of the 103 local responses. This is done by selecting each required local response to be included in the averaging. A common mode of presentation is amplitudes in concentric rings around the center (ring averages). For this analysis, we chose to average the amplitudes for all local responses along diagonal axes, corresponding to the diagonal axes of the extent of subretinal fluid for a given lesion.

Lesion size was measured with calipers on the fundus photography which was obtained simultaneously with the SD-OCT recording. The extent of subretinal fluid along each diagonal axis defined lesion size. In all patients thus analyzed, the constant OCT findings along these diagonals were: 1) subretinal fluid 2) precipitate-like abnormalities at the level of the photoreceptor outer segments. With the Spectralis SD-OCT software, there is a point to point correspondence between the SD-OCT scan and the fundus image. The fundus diagonal was measured across the area that featured precipitate-like abnormalities at the level of the outer segments and subretinal fluid, crossing the point of fixation (fovea). Thus for each lesion, we obtain two SD-OCT -guided fundus photographic measures of lesion size, and two mfERG measures, one for each diagonal. The principles of measurement of lesion diagonal and corresponding mfERG averaging are presented in Figure 1.

To validate that the diagonal measurements between the extent of subretinal fluid (lesion size) and the mfERG measurements were in accordance, i.e. at the same anatomic location, we used infrared camera fundus monitoring during the mfERG recording, a relatively recent feature of the mfERG VERIS equipment. Thus fixation could be assessed during the recording, and segments of the recordings that featured poor fixation were discarded and re-recorded. Furthermore, there is only one way to obtain a linear diagonal of adjacent hexagons crossing and including the central hexagon, i.e. these diagonals will be given unambiguously (Fig. 1). The OCT guided fundus photographic measurements of lesion size were subsequently obtained across the foveal fixation point, at axes corresponding to those defined by the mfERG diagonals, as judged from anatomic landmarks e.g. blood vessels, present on the fundus infrared camera monitoring during mfERG registration. The OCT-based fundus photographic measurements of lesion size were obtained manually with calipers by two observers, independently, according to the above.

The analysis included both eyes of five patients (age range 38-55 years) with the genotypes p.Asn99His, p.Asp302Asn (two patients), p.Leu20Val, and p. Asn296Ser, resulting in a total of ten eyes or 20 points of measurement (corresponding to the two diagonal axes for each lesion). A further two right eyes of two patients aged 25 and 54, with mutation p.Asn296Ser, were also included. These patients were the ones in whom we had data from both modalities (mfERG and SD-OCT) and in whom subretinal fluid was found along with photoreceptor abnormalities. Most of these eyes were in a clinical stage equivalent to the vitelliruptive stage, and all demonstrated variable amounts of subretinal fluid accumulation.

As a secondary outcome measure, mfERG central amplitudes (rings 1-2), lesion size, EOG value, foveal thickness, height of subretinal fluid and age were analyzed for correlation with visual acuity.

Statistical analysis of correlation was carried out with Spearman´s rank correlation (SPSS 16 [originally, Statistical Package for the Social Sciences, IBM, Armonk, New York, USA]).

Molecular genetic methods

DNA was extracted from the peripheral blood samples collected from members of eight families and one isolated case. *BEST1* exons as well as the flanking intronic regions were amplified by standard PCR followed by direct sequencing of the corresponding fragments. Primer sequences for *BEST1* amplification from genomic DNA were previously reported as follows: exons 2-3 and 5-11 (6) and exon 4.[4]

To estimate the pathogenicity of novel missense changes, we used the following *in-silico* tools: Polyphen-2 (http://genetics.bwh.harvard.edu/pph2/index.shtml) and MutationTaster (http://neurocore.charite.de/MutationTaster/index.html).

Results

Minimum prevalence estimate of Best disease in Denmark

In all, we identified 45 individuals with Best disease born between 1924 and 2002 and living on January 1, 2011, in whom a *BEST1* mutation was found previously or in the present study. The corresponding prevalence rate was 0.8:100,000. Selecting individuals born in the 25-year period 1961 through 1985 in which the registration was most complete corresponded to a birth prevalence rate of 1.5:100.000 (26 cases in 1,726,407 live births). Most cases (43 out of 45) belonged to families with 2-8 affected individuals: Fifteen such families were identified (Table 1).

Mutation analysis

Mutations in *BEST1* identified in Danish families in the present study and in previous studies are summarized in Tables 1 and 2.[8,11-16] In the present study, sequencing analysis of all *BEST1* exons revealed heterozygous missense changes that are likely pathogenic in all eight analyzed families as well as one sporadic case (Fig. 2, Supplemental material at AJO.com or Supplemental Fig. 1, and Table 1). Two of the six mutations we identified have been previously described in patients with Best disease: p.Asn296Ser was reported in one patient,[14] and was identified in this study in an index patient and her affected son (family VMD20107) and p.Asp302Ala,[15] that we identified in an index patient and her affected son (family VMD20109). The remaining four mutations were not reported thus far (Table 1, which includes Danish families and mutations reported earlier): p.Leu20Val (in the index case of VMD20110), p.Gln96Arg (in the index case of VMD20112, a father of Turkish descent and his daughter. The p.Gln96Arg mutation was also found in an unrelated sporadic case, VMD24003, but never published [Bakall B. personal communication 1999]), p.Asn99His (in an isolated case from family VMD24004), and p.Asp302Asn (identified in four apparently unrelated families: VMD20102, VMD20105, VMD20106 and VMD24005, Table 2). Genealogical tracing of ancestors back to about 1800 did not show any links between these four families, which however clustered around a few neighbouring parishes, which makes it possible that p.Asp302Asn indeed is a founder mutation.

To estimate the pathogenicity of these missense changes, we evaluated the conservation of the affected residues during evolution, the presence of mutations affecting adjacent residues or even the same residue, and we performed an *in-silico* analysis using Polyphen-2 and MutationTaster (Table 1). Three of the four residues affected by the novel mutations are perfectly conserved during

evolution (Fig. 3) while Asn99 is moderately conserved, but never replaced by histidine. In addition, mutations were already reported to affect many amino acid residues that are adjacent to the four residues affected by novel missense mutations that we describe here (Fig. 3). Moreover, mutations are already known to affect two of the four residues (Asn99 by one mutation and Asp302 by three different missense mutations). Analysis by Polyphen-2 and MutationTaster revealed a high score for the effect on protein function for three of the four mutations, while a low score was obtained for p.Asn99His (Table 1). We therefore suggest that three (p.Leu20Val, p.Asp302Asn, and p.Asp302Ala) of the four mutations are likely pathogenic while p.Asn99His is possibly pathogenic. No family members were available to verify the segregation of this mutation in the corresponding families.

Clinical evaluation

Clinical data in patients with Best disease identified in the present study are presented in Table 2. Considering all identified patients including previous studies, we found a median age-of-onset in Best disease of 19 years (range 4-65). In the present study, the size of the vitelliform lesion exceeded half a disc diameter in all patients except in two patients in whom both eyes had lesions smaller than a half disc diameter.

We aimed at clinical follow-up in the 10 patients, in whom a molecular genetic diagnosis was confirmed only recently by us (as presented in this paper in Table 2). Eight of these accepted a follow-up exam, including optical coherence tomography, fundus autofluorescence imaging and mfERG. Thus 16 eyes of eight patients were examined by these modalities at follow-up, except for mfERG which was not possible in the youngest patient #78503 age 10 and was performed only in the right eye of #76972 and her son, thus resulting in a total of 12 eyes examined by mfERG.

Best corrected visual acuities in the best eye ranged between 0.1 and 0.9 and in the worst eye between 0.05 and 0.8 (Table 2). All but two patients demonstrated stability or decline of visual acuity over follow-up (follow-up range 10-55 years, Table 2). The two exceptions in whom a seeming improvement of vision was seen included a boy in whom the first examination was performed at the age of 10 (son of 76972, with the p.Asn296Asr mutation) and may thus have been flawed by problems with cooperation, and a woman (78502, age 37, p.Asp302Asn) in whom follow up period was only a few months, giving the impression of measurement error (Table 2). However, it has been recently demonstrated that relatively short term fluctuations in visual function may occur in Best disease or in autosomal recessive bestrophinopathy (ARB), in association with subretinal fluid accumulation.[17]

A clinical analysis of retinal function and structure at recent follow-up revealed variable degrees of central dysfunction and structural alterations ranging from abnormalities of photoreceptor outer segments, the extent of which corresponded to subretinal fluid accumulation, and inferior accumulation of subretinal hyperautofluorescent alterations (Supplemental material at AJO.com or Supplemental Figs. 2,3), to choroidal neovascularization with cystoid macular edema. The latter was found in the right eye of a 10-year-old patient, family VMD200035, heterozygous for *BEST1* p.Asp302Asn. The choroidal neovascularization was treated with a single intravitreal injection of 0.5 mg Ranibizumab and photodynamic therapy with Verteporfin, leading to resolution of macular edema and improvement of vision (Table 2). The mother of the patient (78502, Table 2) carried the same mutation in *BEST1* and was asymptomatic with normal visual acuity, normal amplitudes of the mfERG despite multifocal vitelliform changes in the retina.

In the other families that have been described previously, the phenotypes were compatible with earlier descriptions of the phenotype. None of the patients had angle closure glaucoma which

may be associated with Best disease or ARB.[5,17] The youngest individual presenting with subtle retinal structural alterations due to Best disease was four years of age, described by us previously.[16]

Fundus autofluorescence demonstrated hyperautofluorescence of accumulated material on Bruch´s membrane and of the precipitate-like alterations at the level of the photoreceptor outer segments that were found to be associated with subretinal fluid (Supplemental material at AJO.com or Supplemental Figs. 2,3). Autofluorescence in the left eye of the youngest patient aged 10 years was relatively homogeneous, however SD-OCT demonstrated accumulation of subretinal material in an inferior location which corresponded to localized inferior hyperautofluorescence. In all other patients, autofluorescence was granular with predominantly inferior accumulation of hyperautofluorescence, corresponding to hyperreflective subretinal accumulation at the level of the photoreceptor outer segments and on Bruch´s membrane, as imaged by SD-OCT, similar to that presented as Supplemental material at AJO.com or Supplemental Figs.2,3.

There was a significant negative correlation between the extent of photoreceptor abnormalities (that coincided with the extent of subretinal fluid) and retinal function ($p=0.007$, Spearman´s rho correlation coefficient =-0.533, two-tailed Spearman´s rank correlation, Fig. 4). To correct for a possible bias due to correlation between the lesion diagonal diameters for a given lesion, we averaged these as a single estimate of lesion size for a given lesion (presented explicitly in Table 2), and tested for correlation with an average of the two mfERG measures for a given lesion, described above. This resulted in correlation $p=0.013$, rho=-0.692. The same measurements were repeated with SD-OCT guided measurements of lesion size obtained by caliper measurement by a second observer, with similar significant results ($p<0.05$ for both measures). Finally, to correct for a possible bias due to correlation between paired eyes, we analyzed only right eyes of patients, with similar findings for both observers ($p=0.026$ and $p=0.05$, respectively for the two observers).

As a secondary outcome measure, we analyzed for potential correlation between age, EOG values, foveal thickness, height of subfoveal fluid, lesion size and mfERG central (rings 1-2) amplitudes versus visual acuity. Of these factors, mfERG central amplitudes (rings 1-2) were significantly correlated with the logarithm of the minimum angle of resolution visual acuity ($p=0.012$, Spearman´s rho= -0.643, respectively, Table 3). The latter correlation was also demonstrated by us previously in Best disease.[8]

Discussion

Generally, age at onset in Best disease is below 40 years.[18] The real age at onset is, however, mostly unknown due to a pre-symptomatic period of unknown duration postponing the "age at onset" to the age at the first examination. Among all identified Danish patients, we found a median age-at-onset in Best disease of 19 years (range 4-65). EOG Arden ratios are usually considered the most specific clinical diagnostic measure of Best disease with values typically less than 1.5. Yet, values around 1.5 are ambiguous, and convincing Best disease cases with normal Arden ratios have been reported.[8,19] Familial occurrence, with at least one relative affected, was seen in all families described, except in two families (Fig. 2).

In a previous estimate of the prevalence of Best disease carried out in Northern Sweden estimating a prevalence of 2 per 10,000.[7] In that study, which was performed long before the identification of *BEST1* as the gene underlying Best disease in 1998,[12] prevalence estimate was based on 95 identified cases, 75 of whom belonged to a single family. The prevalence estimate found in our study is more than 10 times lower, which underscores the influence of founder mutations and large families on national prevalence rates. It may be anticipated that the condition is under-diagnosed due to failure of recognition of the variable phenotype, reduced expression, and asymptomatic cases, which may account for a considerable proportion of the total number of

prevalent cases. For comparison, the prevalence of Stargardt disease, which is considered as the most common hereditary macular dystrophy with juvenile onset, was estimated to 1 in 8,000 to 10,000.[20]

Ideally, a prevalence study should be prospective and population-based. However, Best disease is relatively rare and thus a very large amount of individuals would need to be examined over a long period of time in order to reach a representative prevalence estimate. Furthermore, molecular genetic testing and clinical electrophysiological investigations are time consuming and costly. This approach was therefore not possible. Our approach was that of a retrospective analysis of all identified patients at a single national referral center, in relation to an estimate of the size of the general population. Causative mutations were identified in all affected patients from whom DNA was available.

Genetic analyses performed in the present study included a further eight families and one sporadic case not reported earlier. *BEST1* missense mutations were found in all. Four mutations are novel; c.904G>T (p.Asp302Asn) was identified in members of four different families while p.Leu20Val, Gln96Arg, and p.Asn99His were identified each in a single family (Tables 1-2). Additional data is required to determine if the p.Asn99His missense change is indeed a pathogenic mutation. Four mutations were described by us previously (Table 1, Family DI-IV).[8] Two additional Danish families were reported by Bakall et al. in 1999 (Table 1).[11]

Patients with Best disease identified in the present study demonstrated a variable clinical appearance, ranging from precipitate-like alterations at the level of the photoreceptor outer segments to choroidal neovascularization. The findings thus exceeded those reported recently in asymptomatic patients with Best disease, in whom a subtle thickening was demonstrated by SD-OCT between the retinal pigment epithelium and the photoreceptors.[21]

Bestrophin is expressed in the retinal pigment epithelium and mutations in *BEST1* lead frequently to the accumulation of subretinal fluid, presumably due to failure of the retinal pigment epithelium pump function, which is the primary mechanism keeping the subretinal space free from fluid in the physiological state.[22] Abnormalities of the photoreceptor outer segments were found over lesions featuring subretinal fluid, the extent of which correlated with the reduction of retinal function over these lesions (Figs. 1,4 and Supplemental material at AJO.com or Supplemental Figs. 2,3). These abnormalities were hyperautofluorescent, similar to those seen in central serous retinopathy.[23] Furthermore, similar findings have recently been described in vitelliruptive and pseudohypopyon stages of Best disease,[24] in young patients with ARB,[25] as well as in Canine Multifocal Retinopathy (Zangerl B, et al. IOVS 2011;52 ARVO E-Abstract 2160), an animal model of Best disease.[9] The structural basis of this finding is not clear at present, but may reflect an impaired turnover of photoreceptor outer segements, leading to their accumulation as precipitates, similar to that recently described in central serous retinopathy by Maruko et al., where these subretinal precipitates were seen to acquire autofluorescence over time.[23]

The progression of OCT and fundus autofluorescence findings in central serous retinopathy were described by Spaide.[26] It was suggested that elongation of photoreceptor outer segments result in progressive hyperautofluorescence. With time autofluorescence becomes granular, possibly due to macrophage accumulation on the surface of the outer retina and in the subretinal space. In late stages, as the retinal pigment epithelium is dying, the autofluorescence is reduced. In the present study however, patients with Best disease were not imaged over time. Nevertheless, we could demonstrate hypoautofluorescence and atrophy in more advanced lesions (Supplemental material at AJO.com or Supplemental Fig. 3). It seems that further comparison of the pathogenesis of Best disease and central serous will require longitudinal studies, for example to enable a comparison of progression of morphological alterations over time.

Various rearrangements of the mfERG array to study the relationship between function and structure have been performed previously in the study of, for example, diabetic retinopathy and rhegmatogenous retinal detachment.[27,28] We used averaging of adjacent hexagons along the two diagonal meridians crossing and including the central foveal hexagon. These diagonals are given unambigously. The infrared fundus illumination during mfERG recording allows for fixation control and allowed as to align these diagonals with corresponding diagonals in the fundus image of the Spectralis SD-OCT, obtained simultaneously with acquisition of SD-OCT. The lesion extent across the Spectralis fundus image was measured with calipers along these diagonals, given by the extent of subretinal fluid at these axes. In this cohort, the extent of subretinal fluid along these axes coincided with the extent of precipitate-like abnormalities at the level of the photoreceptor outer segments.

Our analysis of correlation between lesion diagonal dimension and mfERG diagonal amplitude average in Best disease has several potential limitations. For example, the anatomical location of the mfERG and OCT recording may have been further improved utilizing software for overlay of the fundus picture obtained during mfERG, onto the one obtained during SD-OCT, so as to enable exact and systematic correspondence of anatomy. Sample size was limited (seven patients). Due to these limitations, we suggest that this finding in the present paper should be interpreted as hypothesis generating, implying a specific relation between function and structure in stages of Best disease featuring subretinal fluid. The methodology may be valid in further studies, for example to evaluate outcomes of future gene therapy. Further investigation, including improved alignment of anatomical location between mfERG and OCT recording, is needed to establish the method.

In summary we describe outer retinal structural alterations in Best disease, the extent of which was associated with reduced retinal function, thus potentially leading to further visual compromise. If, as suggested by our data, these changes represent a secondary pathogenetic event in Best disease due to the presence of long standing subretinal fluid, then SD-OCT and mfERG may be valid investigations in finding a therapeutic window and monitoring outcomes of future gene therapy for Best disease.

Acknowledgements:
a. Funding/support: Grants from the Swedish Society of Medicine, Eye Foundation, Dag Lenard Foundation, Foundation for the Visually Impaired in the Skane County, Crownprincess Margareta´s Foundation for the Visually Imparied and grant no. 3000003241 from the Chief Scientist Office of the Ministry of Health, Israel.
b. Financial disclosures: None of the authors have any financial interest to disclose.
c. Contributions to Authors:
Design of the study (HB, PS, DS, TR).
Conduct of the study (HB, PS, LM, TR).
Collection, management, analysis, and interpretation of the data (HB, PS, LM, DS, TR).
Preparation, review and approval of the manuscript (HB, PS, LM, DS, TR).
d. Prospective Institutional Review Board approval obtained at the Lund University Review Board, Lund, Sweden. Proper informed consent for participation in the research was obtained. The study was adherent to the Declaration of Helsinki. The authors (HB, PS, LM, DS, TR) confirm that they are in compliance with their Institutional Review Boards.
e) Other acknowledgement: We appreciate the genealogical investigations carried out by Mr. Erik Kann (National eye clinic, Kennedy Center, Glostrup, Denmark), the independent lesion size measurements on Spectralis optical coherence tomography scans by Mads Kofod, MD (Department of Ophthalmology, Glotrup Hospital, Glostrup, Denmark), the technical assistance in preparation of figures by Mr. Johnny Ring (Department of Ophthalmology, Skane County University Hospital, Malmo, Sweden) and the statistical expertise by Mr. Bo Friberg (Skane County Counsil for research and development, Malmo, Sweden).

References:

1. MacDonald IM, Lee T. Best Vitelliform Macular Dystrophy. In: GeneReviews [Internet]. Available at http://www.ncbi.nlm.nih.gov/books/NBK1167/. Accessed May 10, 2011.
2. Iannaccone A, Kerr NC, Kinnick TR, Calzada JI, Stone EM. Autosomal recessive best vitelliform macular dystrophy: report of a family and management of early-onset neovascular complications. Arch Ophthalmol 2011;129(2):211-217.
3. Kinnick TR, Mullins RF, Dev S, et al. Autosomal recessive vitelliform macular dystrophy in a large cohort of vitelliform macular dystrophy patients. Retina 2011;31(3):581-595.
4. Bitner H, Mizrahi-Meissonnier L, Griefner G, Erdinest I, Sharon D, Banin E. A Homozygous Frameshift Mutation in BEST1 Causes the Classical Form of Best Disease in an Autosomal Recessive Mode. Invest Ophthalmol Vis Sci 2011;52(8):5332-5338.
5. Burgess R, Millar ID, Leroy BP, et al. Biallelic mutation of BEST1 causes a distinct retinopathy in humans. Am J Hum Genet 2008;82(1):19-31.
6. Davidson AE, Millar ID, Urquhart JE, et al. Missense mutations in a retinal pigment epithelium protein, bestrophin-1, cause retinitis pigmentosa. Am J Hum Genet 2009;85(5):581-592.
7. Nordström S. Hereditary macular degeneration - a population survey in the county of Västerbotten, Sweden. Hereditas 1974;78(1):41-62.
8. Schatz P, Bitner H, Sander B, et al. Evaluation of macular structure and function by OCT and electrophysiology in patients with vitelliform macular dystrophy due to mutations in BEST1. Invest Ophthalmol Vis Sci 2010;51(9):4754-4765.
9. Guziewicz KE, Slavik J, Lindauer SJ, Aguirre GD, Zangerl B. Molecular consequences of BEST1 gene mutations in canine multifocal retinopathy predict functional implications for human bestrophinopathies. Invest Ophthalmol Vis Sci 2011;52(7):4497-4505.
10. Schatz P, Ponjavic V, Andreasson S, McGee T, Dryja T, Abrahamson M. Clinical phenotype in a Swedish family with a mutation in the IMPDH1 gene. Ophthalmic Genetics 2005;26(3):119-124.
11. Bakall B, Marknell T, Ingvast S, et al. The mutation spectrum of the bestrophin protein-functional implications. Hum Genet 1999;104(5):383-389.
12. Marquardt A, Stöhr H, Passmore LA, Krämer F, Rivera A, Weber BH. Mutations in a novel gene, VMD2, encoding a protein of unknown properties cause juvenile-onset vitelliform macular dystrophy (Best's disease). Hum Mol Genet 1998;7(9):1517-1525.
13. White K, Marquardt A, Weber BH. VMD2 mutations in vitelliform macular dystrophy (Best disease) and other maculopathies. Hum Mutat 2000;15(4):301-308.
14. Marchant D, Gogat K, Boutboul S, et al. Identification of novel VMD2 gene mutations in patients with best vitelliform macular dystrophy. Hum Mutat 2001;17:235.
15. Chung MM, Oh KT, Streb LM, Kimura AE, Stone EM. Visual outcome following subretinal hemorrhage in Best disease. Retina 2001;21(6):575-580.
16. Piñeiro-Gallego T, Alvarez M, Pereiro I, et al. Clinical evaluation of two consanguineous families with homozygous mutations in BEST1. Mol Vis 2011;17:1607-1617.
17. Wittstrom E, Ekvall S, Schatz P, Bondeson ML, Ponjavic V, Andréasson S. Morphological and functional changes in multifocal vitelliform retinopathy and biallelic mutations in BEST1. Ophthalmic Genet 2011;32(2):83-96.
18. Meunier I, Senechal A, Dhaenens CM, et al. Systematic screening of BEST1 and PRPH2 in juvenile and adult vitelliform macular dystrophies: a rationale for molecular analysis. Ophthalmology 2011;118(6):1130-1136.
19. Schatz P, Klar J, Andréasson S, Ponjavic V, Dahl N. Variant phenotype of Best vitelliform macular dystrophy associated with compound heterozygous mutations in VMD2. Ophthalmic Genet 2006;27(2):51–56.

20. Blacharski PA. Fundus flavimaculatus. In: Newsome DA, editor. Retinal Dystrophies and Degenerations. New York: Raven Press, 1988:135–159.
21. Querques G, Zerbib J, Santacroce R, et al. The spectrum of subclinical Best vitelliform macular dystrophy in subjects with mutations in BEST1 gene.Invest Ophthalmol Vis Sci 2011;52(7):4678-4684.
22. Gamulescu MA, Renner AB, Helbig H. [Clinical manifestations of functional disturbances of the retinal pigment epithelium]. Ophthalmologe 2009;106(4):305-310.
23. Maruko I, Iida T, Ojima A, Sekiryu T. Subretinal dot-like precipitates and yellow material in central serous chorioretinopathy. Retina 2011;31(4):759-765.
24. Ferrara DC, Costa RA, Tsang S, Calucci D, Jorge R, Freund KB. Multimodal fundus imaging in Best vitelliform macular dystrophy. Graefes Arch Clin Exp Ophthalmol 2010;248(10):1377-1386.
25. Borman AD, Davidson AE, O'Sullivan J, et al. Childhood-onset autosomal recessive bestrophinopathy. Arch Ophthalmol 2011;129(8):1088-1093.
26. Spaide R. Autofluorescence from the outer retina and subretinal space: hypothesis and review. Retina 2008;28(1):5-35.
27. Holm K, Ponjavic V, Lövestam-Adrian M. Using multifocal electroretinography hard exudates affect macular function in eyes with diabetic retinopathy. Graefes Arch Clin Exp Ophthalmol 2010;248(9):1241-1247.
28. Schatz P, Holm K, Andréasson S. Retinal function after scleral buckling for recent onset rhegmatogenous retinal detachment: assessment with electroretinography and optical coherence tomography. Retina 2007;27(1):30-36.

Figure captions.

Figure 1. Methodology and principles of analysis of correlation between retinal function and structure in Best disease.

Top left. Corresponding fundus image and an example of caliper measurement across the fundus (along the extent of the two diagonal blue arrows) of the two diagonals of a lesion from a patient with Best disease. Green line indicates the location of the Spectral domain Optical Coherence Tomography (SD-OCT) scan displayed at the top right.

Top right. Spectral domain Optical coherence tomography (SD-OCT) scan demonstrating precipitate-like alterations along the outer retinal surface along with subretinal fluid. The extent of the subretinal fluid across the fundus can be determined by caliper measurement in the fundus image, due to a point to point correlation between the SD-OCT and the fundus image (top left), enabling caliper measurement of diagonal lesion extent (defined as extent of subretinal fluid) in the latter.

Bottom left. Multifocal electroretinography (mfERG) amplitude graph averaged from neighbouring adjacent local responses along both diagonal axes, one graph for each axis. deg^2=degree.

Bottom center and right. Symbolic illustrations of the selected local responses among the 103 local mfERG responses, representing responses from both diagonals that were averaged.

Figure 2. Pedigrees of Danish families with Best disease and *BEST1* mutations identified in this study. M1- p.Asp302Asn, M2- p.Asn296Ser, M3- p.Asp302Ala, M4- p.Leu20Val, M5- p.Gln96Arg, M6- p.Asn99His, + denotes the wild type allele. Gray symbols represent patients who are affected by Best disease by history.

Figure 3. Conservation of amino acids affected by novel *BEST1* missense mutations identified in this study in Danish patients with Best disease.

Amino acids color scheme: red (AVFPMILW) represents small amino acids, blue (DE) represents acidic amino acids, magenta (RK) represents basic amino acids, green (STYHCNGQ) represents hydroxyl + amine + basic amino acids, and gray represents the remaining amino acids. The number of mutations reported to affect each amino acid is depicted above the human protein sequence.

Figure 4. Analysis of the relationship between function and structure in stages of Best disease featuring subretinal fluid. There is a significant correlation between the extent (diagonal dimensions) of precipitate-like alterations at the level of the photoreceptor outer segments seen in association with subretinal fluid and the reduction of mfERG amplitude averages along the corresponding diagonal axes. nV= nanovolt. deg^2=degree. mfERG= Multifocal electroretinography. µm= micrometer.

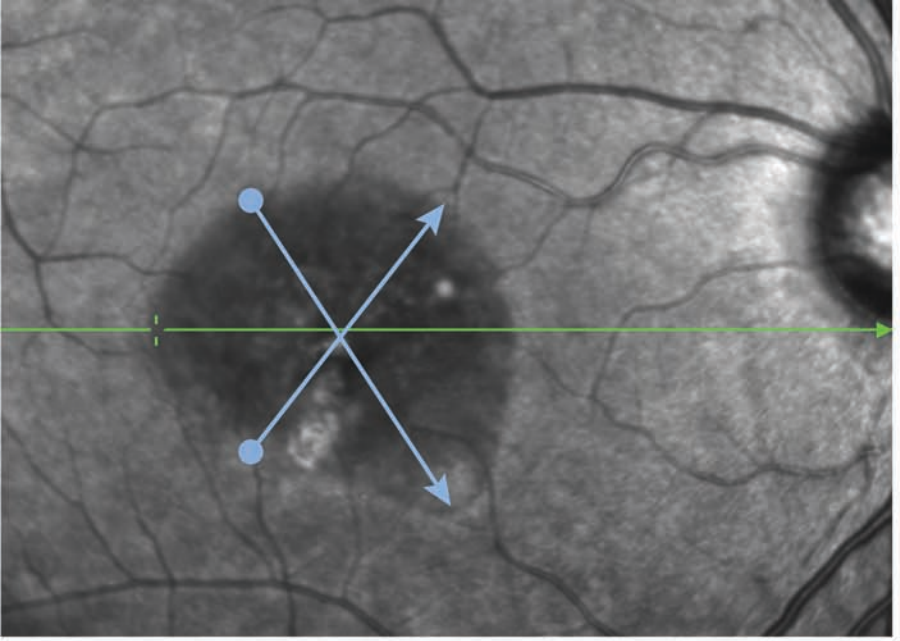

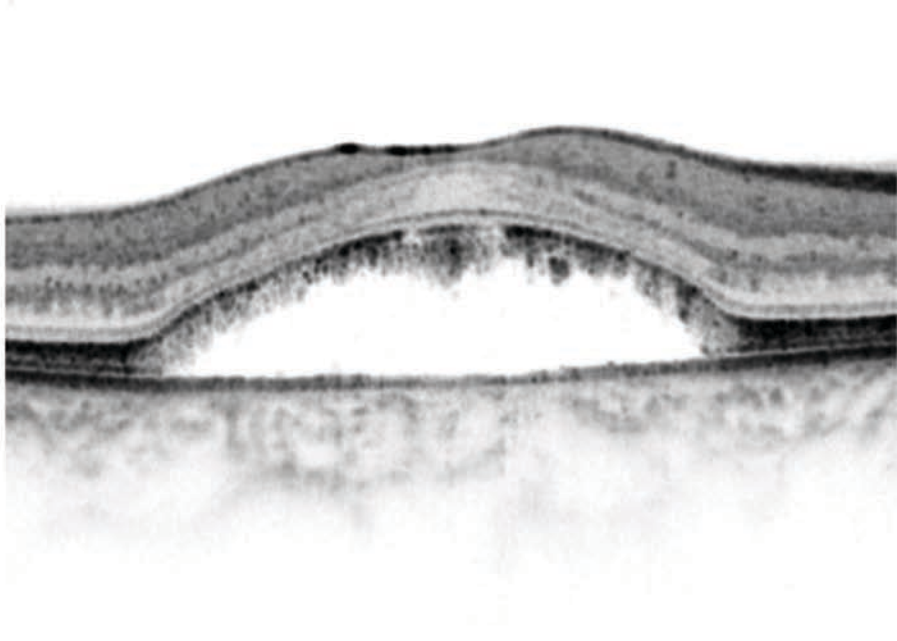

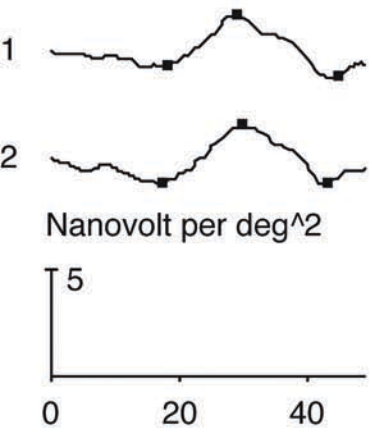
1
2
Nanovolt per deg^2
5
0
20
40
Milliseconds

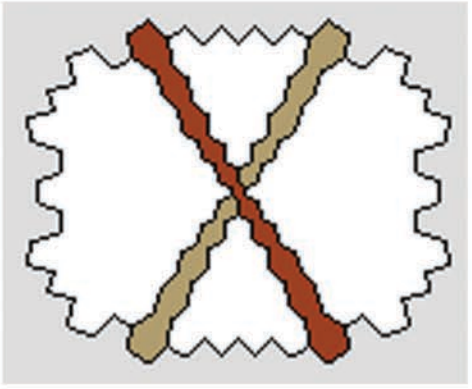

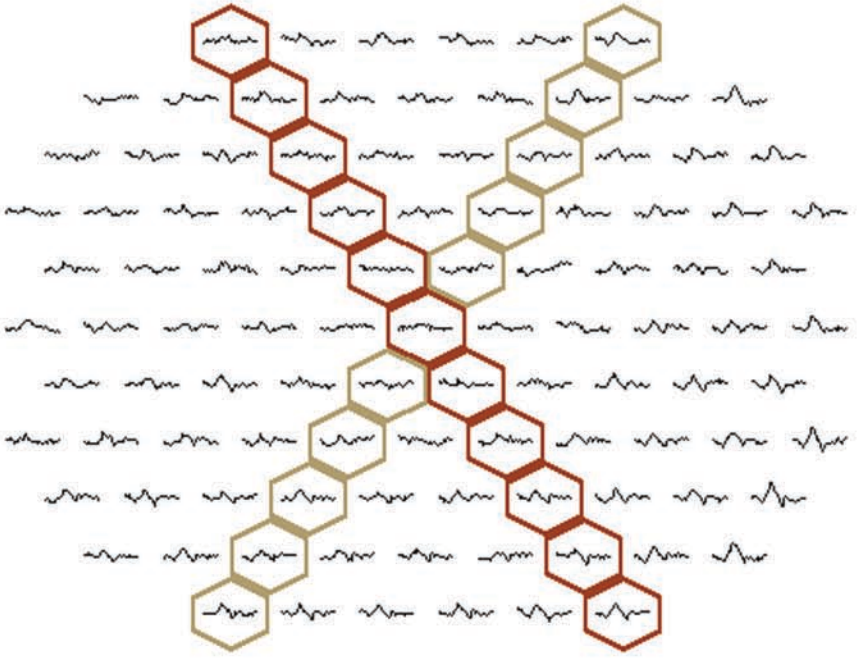

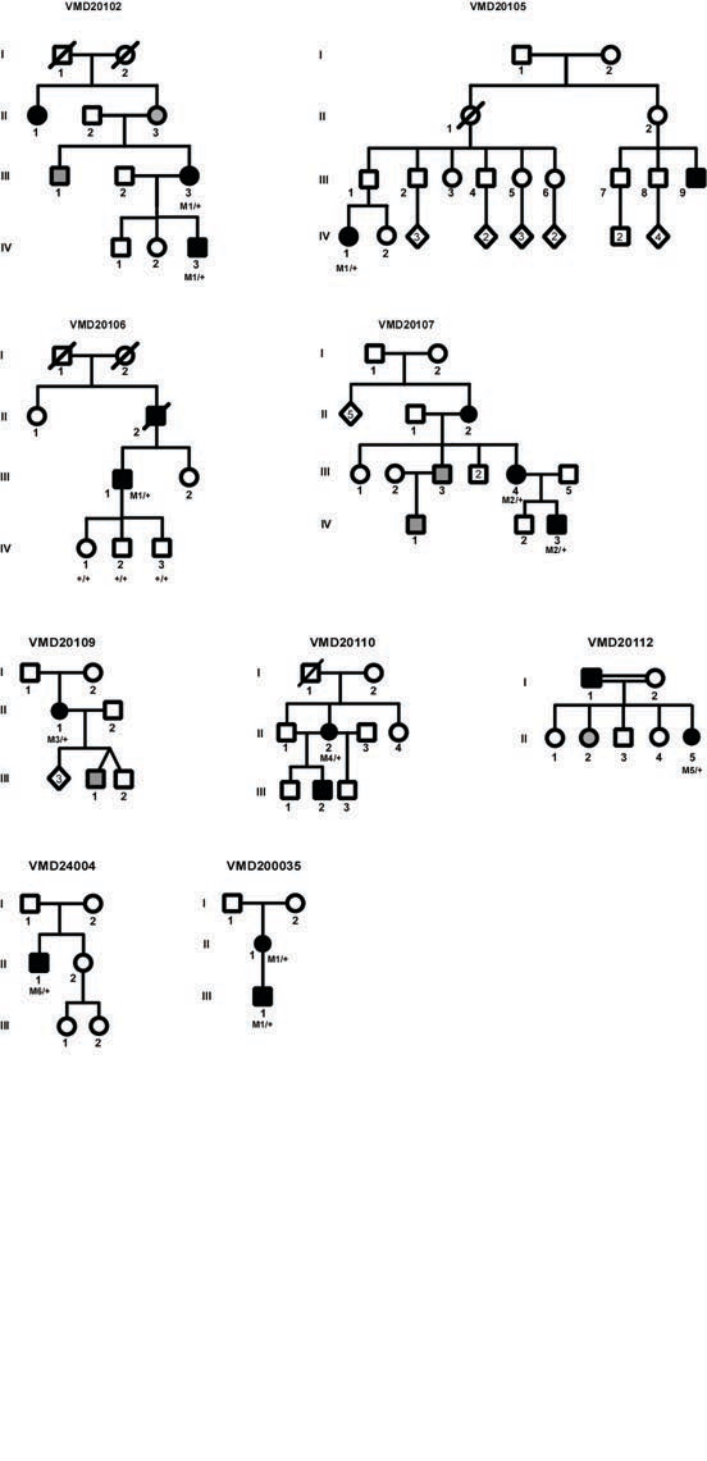
VMD20102
VMD20105
VMD20106
VMD20107
VMD20109
VMD20110
VMD20112
VMD24004
VMD200035

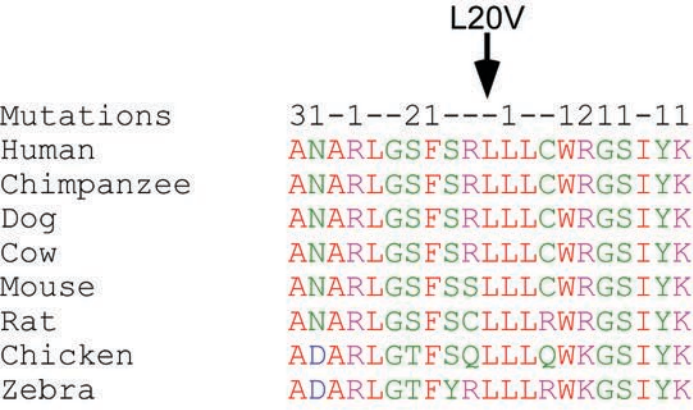
L20V
Mutations 31-1--21---1--1211-11
Human ANARLGSFSRLLLCWRGSIYK
Chimpanzee ANARLGSFSRLLLCWRGSIYK
Dog ANARLGSFSRLLLCWRGSIYK
Cow ANARLGSFSRLLLCWRGSIYK
Mouse ANARLGSFSSLLLCWRGSIYK
Rat ANARLGSFSCLLLRWRGSIYK
Chicken ADARLGTFSQLLLQWKGSIYK
Zebra ADARLGTFYRLLLRWKGSIYK

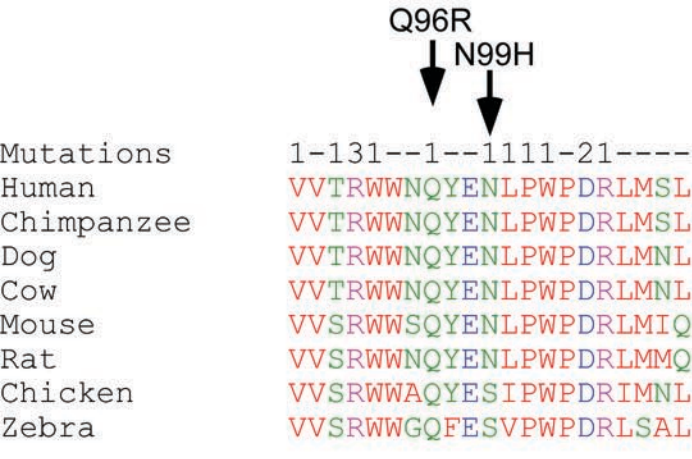
Q96R
N99H
Mutations 1-131--1--1111-21----
Human VVTRWWNQYENLPWPDRLMSL
Chimpanzee VVTRWWNQYENLPWPDRLMSL
Dog VVTRWWNQYENLPWPDRLMNL
Cow VVTRWWNQYENLPWPDRLMNL
Mouse VVSRWWSQYENLPWPDRLMIQ
Rat VVSRWWNQYENLPWPDRLMMQ
Chicken VVSRWWAQYESIPWPDRIMNL
Zebra VVSRWWGQFESVPWPDRLSAL


D302N
D302A
Mutations 2123313243211222-11-
Human QLINPFGEDDDDFETNWIVD
Chimpanzee QLINPFGEDDDDFETNWIVD
Dog QLINPFGEDDDDFETNWIVD
Cow QLINPFGEDDDDFETNWIVD
Mouse QLINPFGEDDDDFETNWIID
Rat QLINPFGEDDDDFETNWIID
Chicken QLINPFGEDDDDFETNWLID
Zebra fish QLINPFGEDDDDFETNWLVD

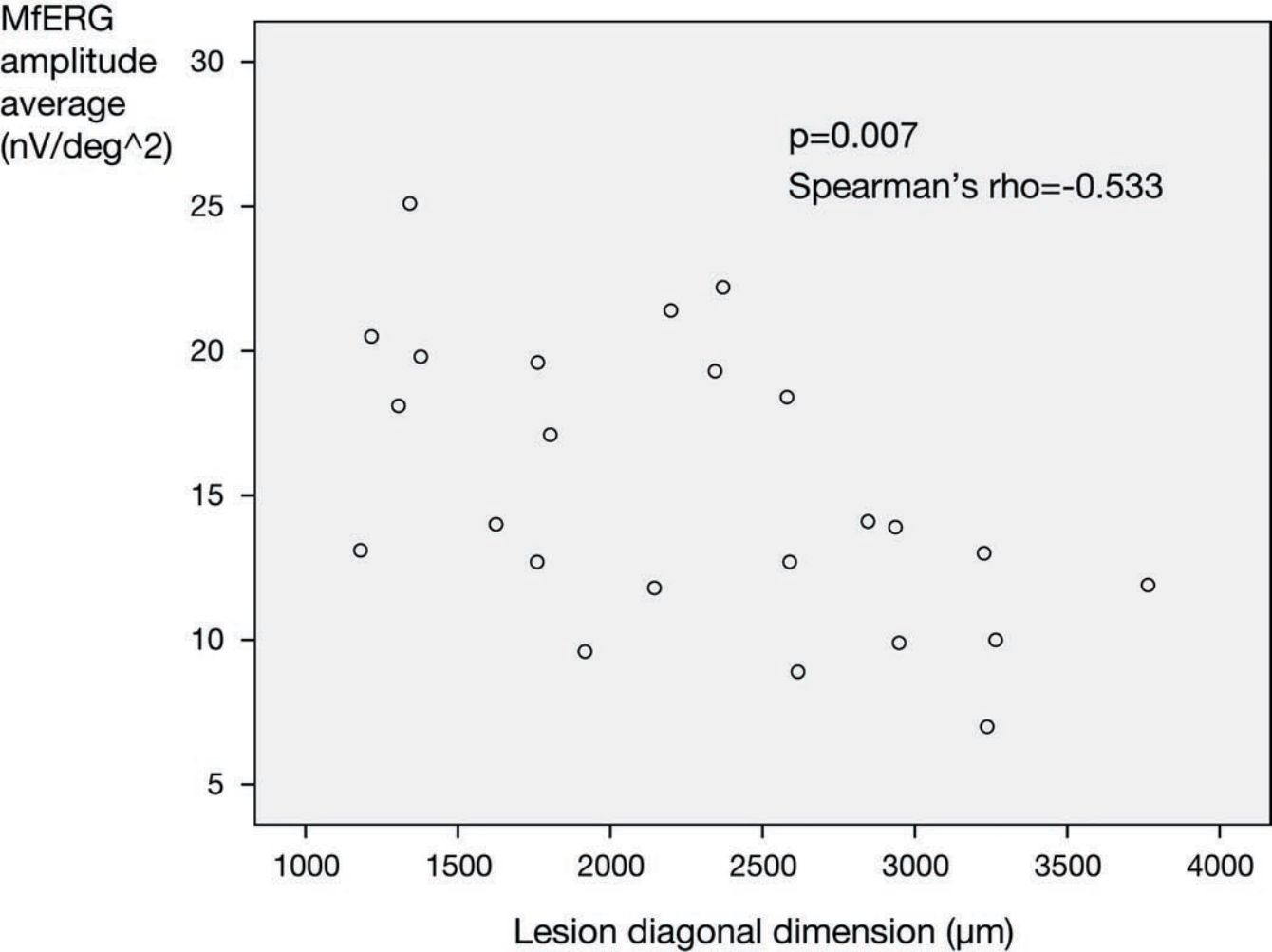
MfERG amplitude average (nV/deg^2)
30
25
20
15
10
5
p=0.007
Spearman's rho=-0.533
1000
1500
2000
2500
3000
3500
4000
Lesion diagonal dimension (µm)

Figure legends supplemental figures

Supplemental Figure 1. Chromatograms of novel BEST1 missense mutations identified in patients with Best disease in this study. The mutated amino acid is marked by an arrow. For each sequence, a wildtype (top) and a heterozygous mutant (bottom) sequence is presented.

Supplemental Figure 2. Individual 56691 with Best disease with the mutation c.295A>C (p.Asn99His) in *BEST1*. Age 41, male. Electro oculography Arden ratio 1.5/1.6. Visual acuity at present 0.8. Left eye. Note hyperautofluorescence (Top right) corresponding to precipitate-like material on the outer surface of the photoreceptor outer segments (Bottom right), and to the focal accumulations on the retinal pigment epithelium / Bruch´s membrane layer. The hyperautofluorescent signal is granular and shows inferior accumulation.

Top left. Fundus.

Top right. Fundus Autofluorescence imaging. Green arrow denotes location of Optical coherence tomography line scan.

Bottom left. Multifocal electroretinography.

Bottom right. Spectral domain Optical coherence tomography.

Supplemental Figure 3. Individual 76976 with Best disease and the mutation c.58C>G (p.Leu20Val) in *BEST1*. Age 50, female. Visual acuity at present 0.05. Right eye. Note paracentral hyperautofluorescence (Top right) corresponding to precipitate-like alterations on the outer surface of the photoreceptor outer segments (Bottom right), and hypoautofluorescence in the center of the lesion, corresponding to atrophy and thinning of the outer nuclear layer. Note focal paracentral accumulation on the retinal pigment epithelium / Bruch´s membrane layer, probably representing some degree of fibrosis.

Top left. Fundus.

Top right. Fundus Autofluorescence imaging. Green arrow denotes location of Optical coherence tomography line scan.

Bottom left. Multifocal electroretinography.

Bottom right. Spectral domain Optical coherence tomography.

VMD20110
c.58C>G
p.Leu20Val

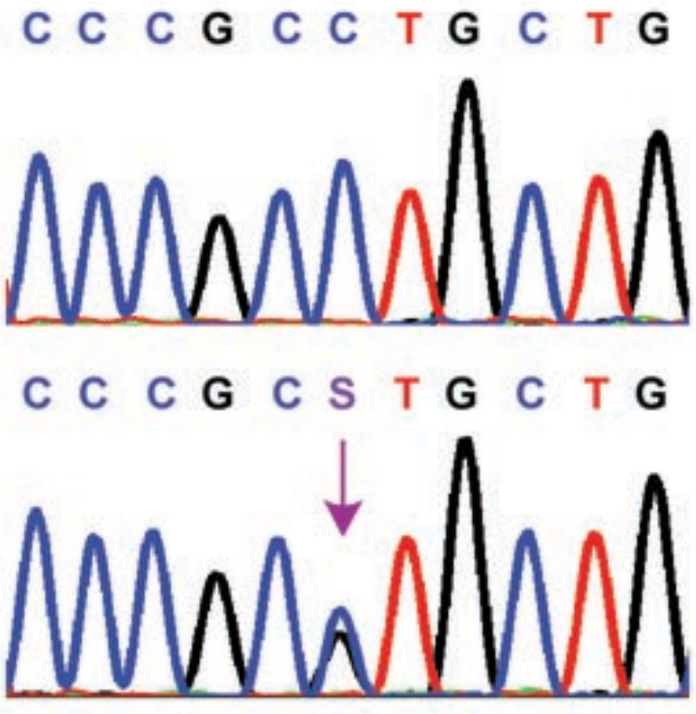

VMD20112
c.287A>G
p.Gln96Arg

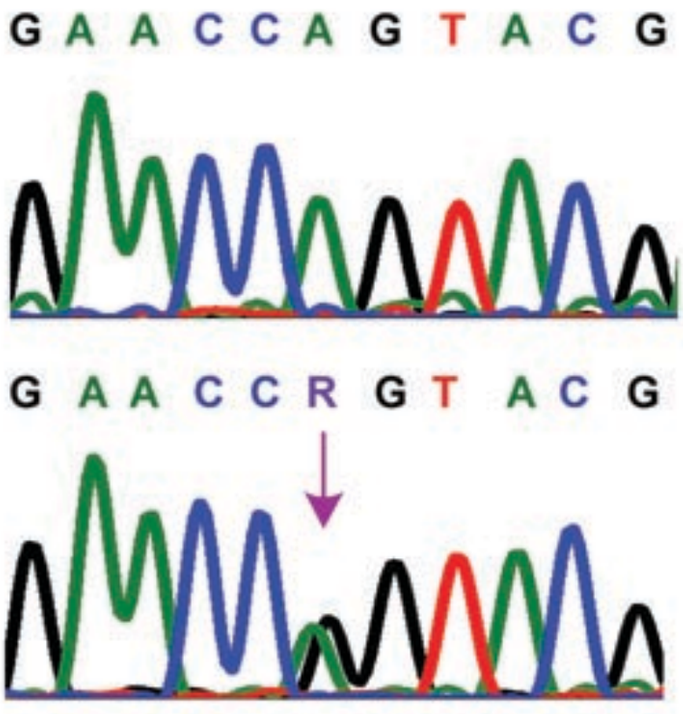

VMD24004
c.295A>C
p.Asn99His

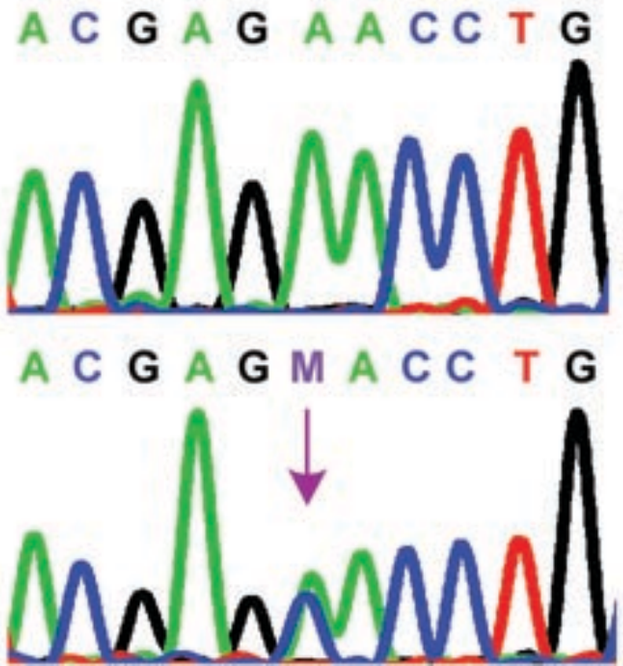

VMD20102, VMD20105, VMD20106, VMD200035
c.904G>T
p.Asp302Asn

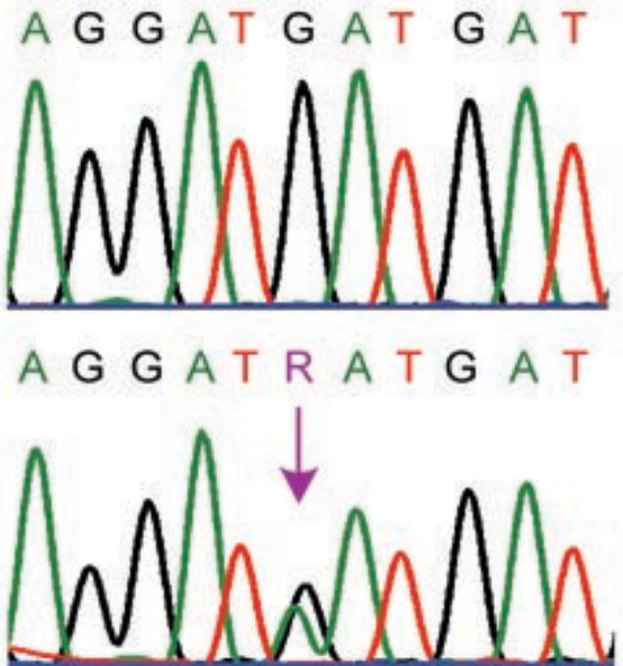

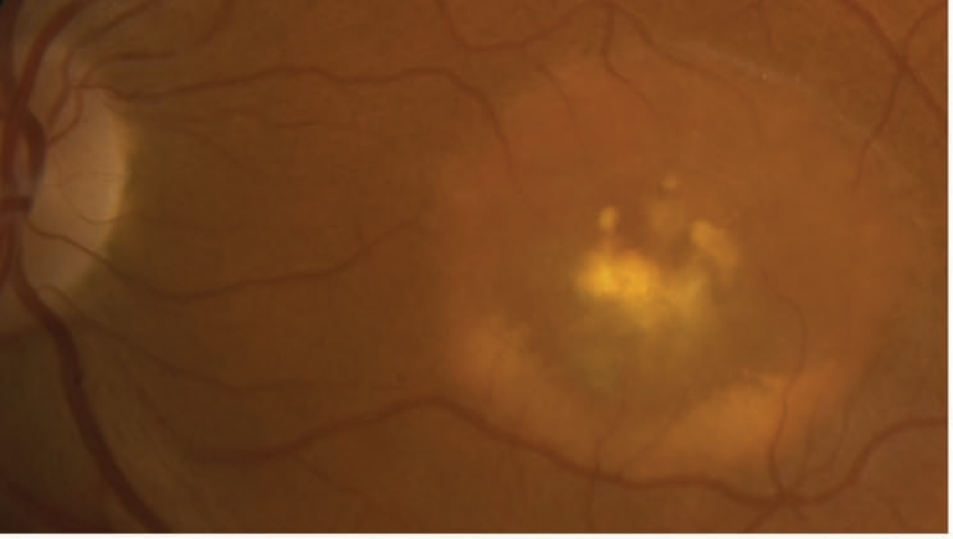

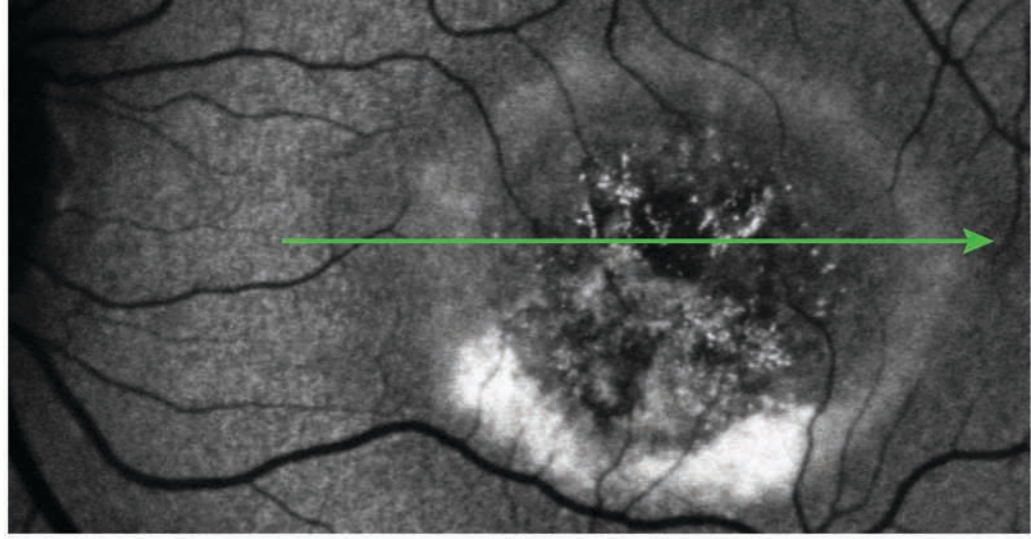

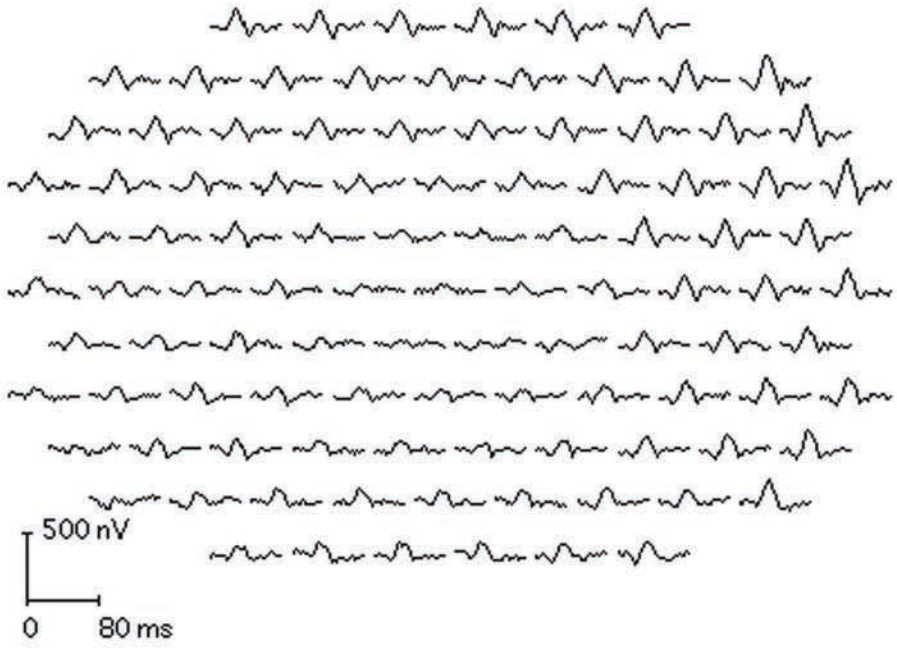
500 nV
0
80 ms

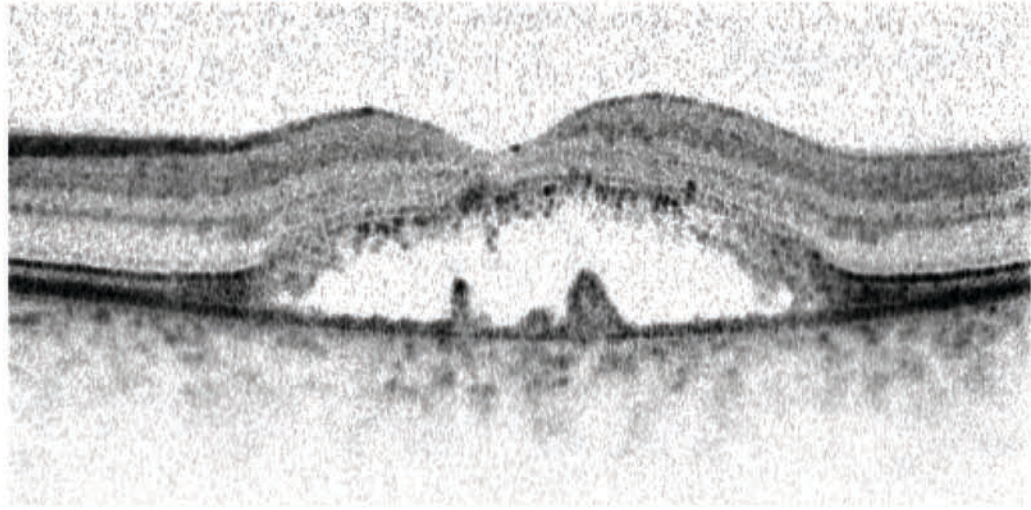

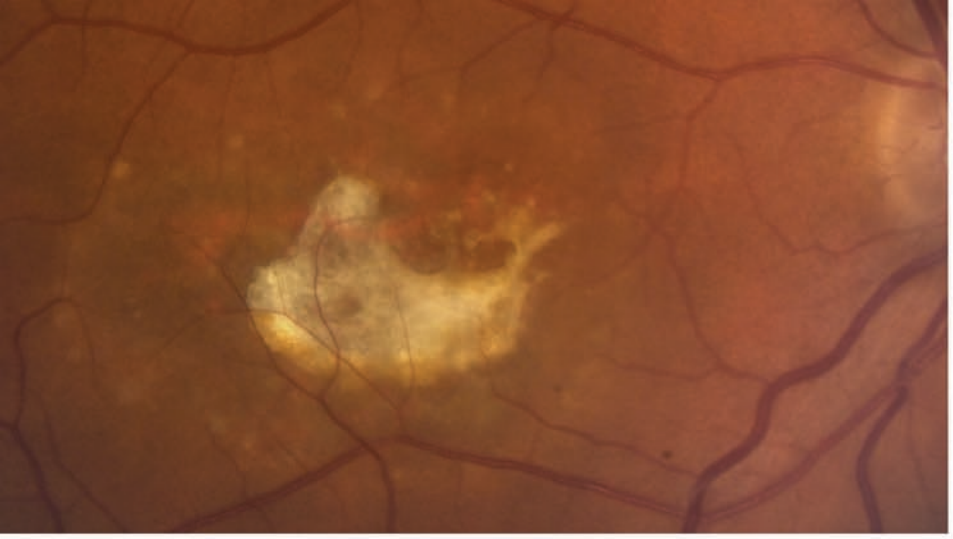

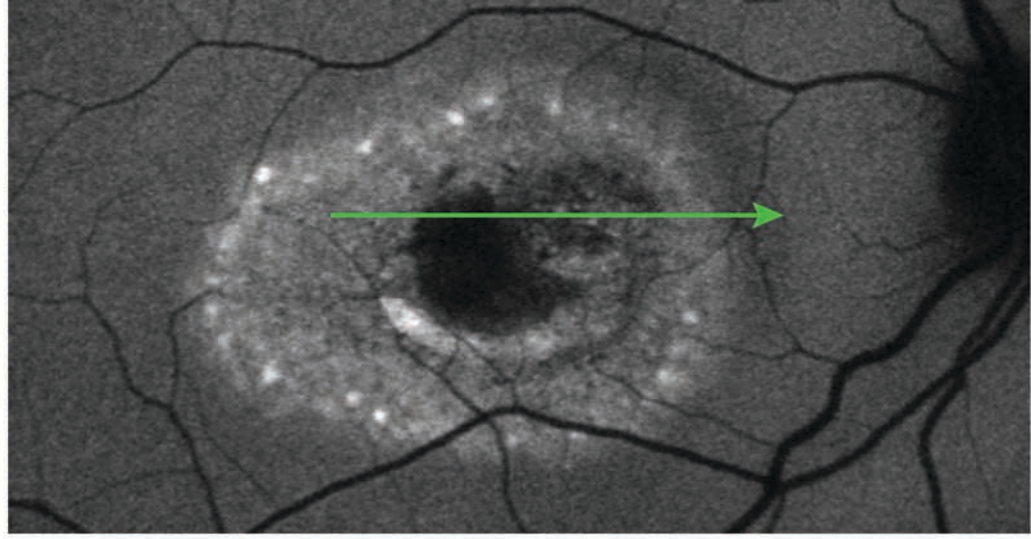

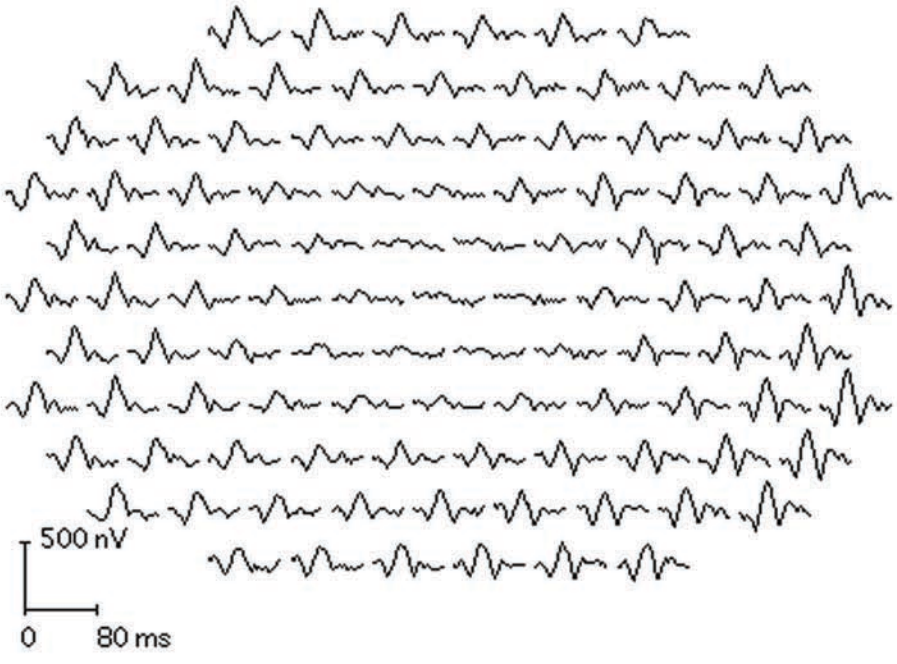
500 nV
0
80 ms

Table 1. Mutation findings including reference to original description of mutation in all known Danish families with Best disease analyzed for mutations in *BEST1*.

***BEST1* mutation (effect on protein)**	**Exon**	**Polyphen-2 prediction (score)**[a]	**MutationTaster prediction (probability)**[b]	**Family**	**Reference**
c.58C>G (p.Leu20Val)	2	Probably damaging (0.999)	Disease causing (p=0.999)	VMD20110	This study, novel
c. 244C>G (p.Leu82Val)	3	Probably damaging (1.000)	Disease causing (p=0.771)	VMD20108	[8,11] (family DIV)
c.253T>C (p.Tyr85His)	4	Probably damaging (1.000)	Disease causing (p=0.596)	VMD200014	[8] (family DI)
c.275G>A (p.Arg92His)	4	Probably damaging (1.000)	Disease causing (p=0.999)	VMD200034	[8] (family DIII)
c.287A>G (p.Gln96Arg)	4	Probably damaging (1.000)	Disease causing (p=0.979)	VMD24003[c]	Bakall B, 1999[d]
				VMD20112	This study, novel
c.295A>C (p.Asn99His)	4	Benign (0.329)	Polymorphism (p=0.783)	VMD24004[c]	This study, novel
c.652C>T (p.Arg218Cys)	6	Probably damaging (1.000)	Disease causing (0.999)	VMD20101	[12]
c.728C>T (p.Ala243Val)	7	Probably damaging (1.000)	Disease causing (1.000)	VMD200022	[13]
c.887A>G (p.Asn296Ser)	8	Probably damaging (0.992)	Disease causing (p=0.989)	VMD20107	[14] and this study
c.904G>T (p.Asp302Asn)	8	Probably damaging (1.000)	Disease causing (p=0.999)	VMD20102	This study, novel
				VMD20105	This study
				VMD20106	This study

				VMD200035	This study
c.905A>C (p.Asp302Ala)	8	Probably damaging (1.000)	Disease causing (p=0.999)	VMD20109	[15], this study
c.936C>A (p.Asp312Glu)	8	Probably damaging (1.000)	Disease causing (p=0.987)	VMD200038	[8,16] (family DII)

[a]Polyphen2- PolyPhen-2 predicts the functional significance of an allele replacement from its individual features by Naïve Bayes classifier trained using supervised machine-learning with a score ranging from 0 to 1.00.

[b]MutationTaster employs a Bayes classifier to eventually predict the disease potential of an alteration. The p value is the probability of the prediction, i.e. a value close to 1 indicates a high 'security' of the prediction.

[c]sporadic case.

[d]personal communication with Bakall B, 1999.

Table 2. Clinical data regarding patients with Best disease included in the clinical follow-up. Here, "lesion size" refers to the average of the two diagonal lesion dimensions for each eye, as measured by calipers in the Spectralis fundus image. VA=best corrected visual acuity. OD=right eye. OS=left eye. µm=micrometers. N/A= not analyzed.

Patient (family)	**Gender (age)**	***BEST1* mutation (effect on protein)**	**Clinical Findings OD / OS**	**Age at onset (age at first documented, VA OD/VA OS)**	**VA recent exam, OD/OS**	**Lesion size OD/OS (µm)**	**EOG OD/OS Arden ratio**
76968 (VMD20102)	M (35)	c.904G>T (p.Asp302Asn)	Atrophic / Atrophic	16 (16, 0.1 / 0.4)	N/A	N/A	2.8 / 2.8
76970 (VMD20105)	F (35)	c.904G>T (p.Asp302Asn)	Atrophic / Vitelliruptive	23 (23, 0.3 / 0.4)	N/A	N/A	1.7 / 1.4
76971 (VMD20106)	M (66)	c.904G>T (p.Asp302Asn)	Vitelliruptive / Atrophic	9 (9, 0.08 / 0.4)	0.1 / 0.05	2462/3496	1.1 / 1.1
76972 (VMD20107)	F (54)	c.887A>G (p.Asn296Ser)	Vitelliruptive / Vitelliruptive	54 (54, 0.9 / 0.2)	0.9 / 0.2	2718/4597	1.1 / 1.3
son of 76972	M (25)	c.887A>G (p.Asn296Ser)	Vitelliruptive / Vitelliruptive	10 (10, 0.2 / 0.2)	0.6 / 0.7	2285/1637	N/A
76973 (VMD20109)	F (61)	c.905A>C (p.Asp302Ala)	Vitelliruptive / Vitelliruptive	15 (45, 0.4 / 0.4)	0.3 / 0.4	3251/2031	1.0 / 1.0
76976 (VMD20110)	F (50)	c.58C>G (p.Leu20Val)	Fibrotic / Fibrotic	36 (36, 1.0 / 0.8)	0.05 / 0.7	2348/1261	N/A
56691 (VMD24004)	M (41)	c.295A>C (p.Asn99His)	Fibrotic / Vitelliruptive	16 (16, 1.0 / 0.5)	0.8 / 0.8	1403/2782	1.5 / 1.6
78502 (VMD200035)	F (37)	c.904G>T (p.Asp302Asn)	Vitelliruptive / Vitelliruptive	37 (37, 0.8 / 0.4)	0.9 / 0.8	1360/1783	N/A
78503 (VMD200035)	M (10)	c.904G>T (p.Asp302Asn)	Fibrotic / Vitelliform	10 (10, 0.2 / 0.2)	0.2 / 0.2	1963/1165	N/A

Table 3. Secondary outcome measures in patients with Best disease that were followed-up in this study: Age, Electro-oculography (EOG) Arden ratio, foveal thickness, height of subfoveal fluid, lesion size defined as the average of the two diagonal SD-OCT based fundus photographic measures of diagonal lesion extension for a given lesion, and multifocal electroretinography (mfERG) central (rings 1-2) amplitudes versus visual acuity (VA). Of these factors, mfERG central amplitudes were significantly correlated with the logarithm of the minimum angle of resolution visual acuity (LogMAR VA).

Secondary outcome measure versus LogMAR VA	**p value**
Age	p=0.133
EOG Arden ratio	p=0.515
Foveal thickness	p=0.334
Height of subretinal fluid	p=0.658
Lesion size	p=0.093
MfERG central (rings 1-2) amplitude	p=0.012, Spearman´s rho= -0.643